Hindawi
Scientific Programming
Volume 2022, Article ID 9667979, 13 pages
https://doi.org/10.1155/2022/9667979

Research Article

Computer-Aided Analysis of Small Clear Space Intersection Tunnel and Heavy Load Railway Surrounding Rock Structure Dynamic Response Characteristics Analysis under Intelligent Manufacturing

Xiaotian Hao[1,2] **and Hailong Wang**[1,3]

[1]*School of Traffic and Transportation, Shi Jia Zhuang Tiedao University, ShiJiaZhuang 050043, HeBei, China*
[2]*School of Urban Construction Engineering, ChongQing Technology and Business Institute, ChongQing 400052, China*
[3]*School of Civil Engineering, HeBei University of Architecture, Zhangjiakou 075000, HeBei, China*

Correspondence should be addressed to Hailong Wang; bhxt196346@cqtbi.edu.cn

Received 25 June 2022; Revised 30 July 2022; Accepted 20 August 2022; Published 28 September 2022

Academic Editor: Juan Vicente Capella Hernandez

Among many tunnel construction projects, small clear tunnels have been the focus of urban rail transit construction in recent years. The purpose of this research work is to study the dynamic response characteristics of the surrounding rock structure of a heavy-duty railway with a small clearance crossing tunnel. It is proposed to analyze the dynamic response characteristics of the surrounding rock structure through the frequency response function. The vertical acceleration, tensile force, stress, and internal strength of the pipe section are specifically analyzed. The influence of the pipe joint and the assembly method on the dynamic response is also analyzed. The influencing factors of stability are analyzed from buried depth, clear distance, and surrounding rock grade. Studies have shown that the minimum clear distance of crossing tunnels increases nonlinearly with the increase of tunnel depth and gravity, and decreases nonlinearly with the increase of cohesion, internal friction angle, calculated internal friction angle, and lateral pressure coefficient. When other parameters are the same and when the side pressure coefficient is less than 1, the minimum clear distance is larger than that of the side pressure coefficient when it is equal to 1. When the vibration frequency exceeds 100 Hz, the coherence coefficient is basically close to 1, indicating that the frequency response function response result of this section is the most reliable. It is hoped that it can provide a reference for the dynamic stability analysis of the surrounding rock structure of the heavy-duty railway surrounding rock structure and the surrounding stratum and the research of structural vibration reduction technology for the small clearance crossing tunnel in the future.

1. Introduction

Since the beginning of the 21st century, with the continuous improvement of the national economy of the country, population mobility has increased year by year, which has brought great challenges to the country's transportation capacity. As the backbone of passenger transportation, railway transportation is bound to increase railway construction. Due to China's vast territory and complex geographical environment, in order to reduce the mileage of railways and shorten the time to reach the destination, the construction of interchange tunnels is bound to occur. At present, the phenomenon of close space crossing between tunnels is becoming more and more common. The dynamic response mechanism of the train under the vibration load and the transmission law of the tunnel structure is very complicated. The vibration response caused by the train is generally lower than the vibration level that causes structural damage to the building. As the train speed increases, the impact on the surrounding environment also increases, so train vibration has a great impact on the environment and other aspects. Under the long-term influence of the train's

vibration load, the tunnel and its surrounding ground have performance degradation problems. The spatial lateral shield under the action of train vibration load is being studied, and the dynamic response of the tunnel and its transmission law appear to be particularly important.

Since the lining structure is the main load-bearing structure of the tunnel, the impact of the tunnel's vibration response on the lining structure should be fully considered when constructing the tunnel. By studying the impact of train vibration load on the lining structure of the grade-crossing tunnel during the operation period, can not only help in guiding the construction of the grade-crossing tunnel but can also grasp the weak links of the grade-crossing tunnel during the operation period, thereby ensuring the safe passage of trains during the operation period. Therefore, the development of research studies on the three-dimensional crossing tunnel under the train vibration load can provide a certain basis for the planning and construction of rail transit, providing corresponding theoretical references for the scientific design and engineering safety construction of similar projects.

Tunnel shield technology has been widely used in subway construction in many cities. In large cities, tunnels inevitably pass between building foundations and deep bridges. Due to the many limitations of urban space in China, the distance between the two tunnels is relatively short. Therefore, the use of shielding technology to solve the mutual influence of the narrow construction of two tunnels is a technical problem to be solved urgently. Lv et al. analyzed the shield construction project of the two tunnels. The clearance of the tunnel is 2.6 m. The project is located between Tongdewei station and Shangbu station on the northern extension of the Guangzhou metro line 8. The main parameters used in his analysis are tunnel lining deformation and ground settlement. Numerical simulations were carried out for the construction process without and with isolation pile reinforcement. The simulation results were compared with the field monitoring data. The comparison shows that through reinforcement, the deformation of the tunnel lining and ground settlement can be greatly reduced. The impact of subway shield construction on the construction of the first subway tunnel will be greatly reduced, and the deformation and mutual influence of the width of the shield excavation net can also be greatly reduced. But the parameters he used in the analysis were not comprehensive enough for numerical simulation [1]. The construction of short-distance superimposed short-distance tunnels with small clear distances faces two major problems, mainly the influence of the tunnel structure and the superposition of the ground settlement caused by the tunnel construction. Taking the section from Hongling North station to Songgang station of Shenzhen metro line 7 as an example, the use of tunnel layers to reinforce ground joints was discussed. Liu et al. explained the first step of using mobile support trolleys in the first excavation section of the tunnel starting with the pipeline. The segment lining structure is strengthened, and technical measures such as control technology are used in the lead time of the shield tunnel excavation in the later period to effectively control the segment lining deformation and surface settlement and to achieve the expected effect. However, his experimental design for controlling the lining deformation and surface settlement of the segment is too complicated, and it is prone to deviation [2]. The Al-Omari RR study proposes experimental and finite element studies to study the behavior of the piled raft tunnel system in the sand. In the experimental work, a small model was tested in a sandbox, and the load was applied vertically to the raft through a hydraulic Jack. Five configurations of piles were tested in the laboratory. The influence of pile length (L), the number of piles in the group, and the distance between the top of the pile and the top of the tunnel surface (H) on the bearing capacity of the piled tunnel system are studied. The experimental work carried out on the piled raft tunnel system shows that for a constant (H) distance, the bearing capacity of the piled raft model increases with the increase of pile length (L), and for a constant pile length, it decreases with the increase of (H). The obtained results show that the finite element method and experimental modeling are reasonable. But he was unable to fully explain the bearing capacity by studying pile length and distance [3]. Zhang et al. proposed an analytical solution to study the response of existing tunnels caused by the excavation of a new underground tunnel. The existing tunnel was modeled with Timoshenko beams on the Kerr foundation, and the proposed analytical solutions were tested against centrifugal tests and field case studies in the literature. The results showed that the prediction results given by the proposed analysis method were consistent with the experimental test data and the onsite measurement results of the construction site. However, the experimental data collected during the centrifugal test is too large, and errors are prone to appearing in the analysis [4]. During the excavation of the underground powerhouse of Baihetan Hydropower Station, which is still under construction, the collapse of the stress structure control often occurs. In order to study the mechanism of this collapse evolution, Xiao et al. conducted in-situ experiments involving microseismic (MS) monitoring in the left main/auxiliary power chamber. He summarized and introduced the temporal and spatial characteristics of the collapse controlled by the stress structure. Onsite investigations, scanning electron microscopy, and mass spectrometry monitoring were used to investigate the collapse of the typical stress structure control that occurred during the monitoring period. These methods provide consistent results that tensile fracture is the most active rock fracture mechanism during the collapse evolution process controlled by the stressed structure. But the method he provided was not reflected in the process of tensile fracture [5]. He et al. proposed innovative cutting mining technology and column-free pressure relief technology in response to the complex construction technology and high roadway construction cost of the traditional technology of retaining lanes along the road. According to the movement law of the upper layer in the traditional technology of road construction along the ditch, the pressure relief mechanism for maintaining the roof along the ditch is being studied. In addition, taking into account different types of roof conditions, a number of mechanical models of "Enclosure and Bedrock Road Construction" were created, and the design formulas for the support resistance of each pavement were obtained. The results show that the upper roof is better

supported by presliding. This reduces the rotational deformation of the upper roof and reduces the impact load caused by roof cracks. The position of the roof fracture is moved to the side of the road, reducing the length of the roof cantilever beam, thereby reducing the additional load of the roadside support. However, the calculation process of the mechanical model and the designed resistance formula he proposed was too difficult, and further research is needed [6].

The innovation of this study is to deal with the cladding of the tunnel shield section and the dynamic response of the ground under the influence of the train vibration load. Using the indoor model test method, the acceleration response of the tunnel structure and the ground is tested, and the dynamic response characteristics in the time domain and frequency domain are analyzed. Then, the material parameters given to the stratum and structure are calculated. Through the three-dimensional dynamic numerical simulation calculation, the influence law of the dynamic characteristics of the different cross-section tunnels under different traffic conditions is studied, the influence of different influencing factors on the tunnel lining structure is simulated, and the parameter sensitivity analysis is carried out. On this basis, the partition of the influence of different influencing factors on the track bed structure along the track direction is divided; and the antivibration analysis is considered by increasing the thickness of the lining and strengthening the surrounding rock in a certain range.

2. Dynamic Response Characteristics of Heavy-Duty Railway Surrounding Rock Structure in Small Clearance Crossing Tunnel

2.1. Vibration Response of a Three-Dimensional Crossing Tunnel with Small Clearance. Crossing tunnels are typical geotechnical proximity projects. The construction of new tunnels will inevitably break the original rock-soil balance of in-situ stress and can produce additional effects on the existing tunnel structure, affecting the safe operation and even the structure of the existing tunnel safety. The dynamic load received by the small clearance interchange tunnel during the normal operation period is mainly the vibration load generated by the train operation [7]. The running train acts on the rails through the wheels, which in turn generates vibration. Therefore, the accurate expression of train vibration load is a very troublesome problem. When the train is running, the vibration load is applied to the tunnel invert and the tunnel bottom structure through the train wheel and rail, and then the vibration load is further transmitted to the adjacent tunnel through the surrounding rock outside the tunnel when the train is running, and then the space crosses the shield tunnel structure and its surrounding environment. The vibration generated by train operation propagates through the tunnel and surrounding soil and has an impact on the environment. Under the action of long-term train vibration load, the waterproof effect and durability of the railway tunnel structure will be significantly affected, and it will also affect the track's performance, ride comfort, passenger comfort, and normal train operations [8, 9]. The model of the grade-crossing tunnel is shown in Figure 1.

The overlapped tunnels at close distances affect each other significantly under the vibration load of the train. The smaller the clear distance between the two tunnels, the greater is the mutual influence. But for the lining structure, the increase in additional stress caused by train vibration is not large.

Before the dynamic load is applied, the surrounding rock has an initial stress, so the static calculation should be carried out first, followed by the dynamic calculation. The main calculation steps are the following: determine the boundary range of the model, then divide the unit grid to establish a three-dimensional numerical calculation model; and then, set the response static boundary conditions and structural mechanics parameters so as to obtain and analyze the vibration response data of the relevant structure.

2.2. Dynamic Response Characteristics of Surrounding Rock Structure. In order to explore the dynamic response of the heavy-duty railway surrounding the rock structure of the small clearance crossing tunnel, the strain state of the soil remains small under the action of vibration load [10, 11]. Special attention should be paid to the monitoring and measurement of the circumference of the tunnel with a small clear distance, a minimum clear distance, and the position of the tunnel vault, the middle of the invert, and the arch waist [12]. Therefore, the elastic model can be used to study the problem so that a similar relationship satisfies the elastic similarity law. The mechanical behavior of the tunnel structure and the soil can be expressed as

$$\begin{cases} D^r\varepsilon + kp = k\gamma, \\ \varepsilon^r = (\varepsilon_{11}, \varepsilon_{21}, \varepsilon_{22}, \varepsilon_{31}, \varepsilon_{32}). \end{cases} \tag{1}$$

In the formula, ε^r is the stress in all directions and ε is the strain.

$$\begin{cases} k\gamma = Dk\varepsilon, \\ k\varepsilon = Dkp. \end{cases} \tag{2}$$

In the formula, p is the density of the soil and γ is the acceleration due to gravity.

$$\begin{aligned} DE\frac{\partial^4 m^r i}{\partial t^2} + p_b m^r \gamma - p_b m^r k = 0, \\ DT\frac{\partial^2 m^r i}{\partial s^2} + p_b s^r \gamma - p_b s^r T = 0. \end{aligned} \tag{3}$$

Among them, m is a unit vector, s is the unit vector tangent to m, k is the tangent modulus, and T is the matrix that transforms stress into force.

$$D^r = \begin{vmatrix} \frac{\varepsilon}{\varepsilon x_1} 0 0 \frac{\varepsilon}{\varepsilon x_2} 0 \frac{\varepsilon}{\varepsilon x_3} \\ 0 \frac{\varepsilon}{\varepsilon x_2} 0 \frac{\varepsilon}{\varepsilon x_1} \frac{\varepsilon}{\varepsilon x_3} 0 \end{vmatrix}. \tag{4}$$

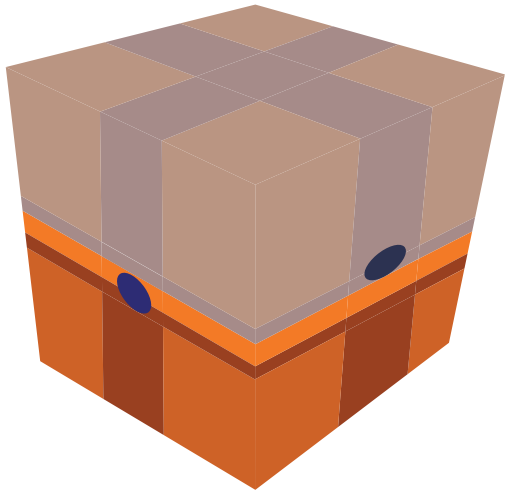

Figure 1: A schematic diagram of the cross-tunnel model.

If k and n are used to represent the physical quantities of the prototype and the model, respectively, then, the similarity ratio between the physical quantities of the model and the prototype can be expressed as

$$\begin{aligned}(d_n) &= g_d(d_k),\ (k_n) = g_n(k_n),\ (E_n),\\ (\varepsilon_n) &= g_\varepsilon(\varepsilon_n),\ (\gamma_k) = g_\gamma(\gamma_n),\ (k_n),\\ (s_n) &= g_s(s_n),\ (\phi_k) = g_n(\phi_n),\ (p_k).\end{aligned} \tag{5}$$

The physical quantities of the soil prototype and the model need to satisfy the balance equation, so they can be transformed into

$$(D^r)_k(\gamma)_n + (p)_k(k)_n = (p)_k(\gamma)_k, \tag{6}$$

$$(D^r)_n(\gamma)_p + (p)_n(k)_p = (p)_p(\gamma)_n. \tag{7}$$

By combining formulas (6) and (7), we get

$$\frac{1}{G_s}(D^r)_n G_\varepsilon(\varepsilon)_n + G_p(p)_n G_k(p)_n = G_p(p)_n. \tag{8}$$

The formula is the similar relationship between different physical quantities. Based on a comprehensive investigation of the functionality and reliability of the experiment, the geometric similarity ratio, the density similarity ratio, and the elasticity coefficient similarity ratio of this experiment are used to meet the similarity ratios of other physical quantities to determine [13, 14].

2.3. The Frequency Response Function. The dynamic response of the tunnel structure and the surrounding ground is not only related to the frequency spectrum characteristics of the vibration load but is also directly related to the amplitude of the applied load [15, 16]. The greater the load amplitude, the more obvious is the dynamic response. When performing dynamic response analysis in the frequency domain, in order to eliminate the influence of the load amplitude on the dynamic response, the frequency response function and the coherence coefficient are used to determine the fixed frequency sinusoidal vibration load and sweep frequency vibration load. The time domain results are processed under different frequency loads, and the dynamic response characteristics of the tunnel structure and the ground environment under different frequency loads are analyzed in detail [17, 18].

When analyzing the dynamic response characteristics in the frequency domain, in order to eliminate the influence of the load amplitude on the dynamic response, this study uses the frequency response function (FRF) and the coherence coefficient to analyze the time domain results under the fixed frequency sinusoidal vibration load and the swept frequency vibration load.

The frequency response function (FRF) is defined as the ratio of the acceleration response after Fourier transformation to the vibration load, which can be expressed as

$$F(\sigma) = \frac{T(\sigma)}{D(\sigma)} + 1. \tag{9}$$

In the formula, the variable $T(\sigma)$ in the frequency response function is the acceleration response and $D(\sigma)$ is the vibration load.

When performing specific calculations, according to the random vibration analysis theory, the data measured in the model experiment is regarded as the random vibration signal. First, the self-power spectral density function of the applied load and acceleration response and the cross-spectral density function between the two are obtained. It can be transformed into two forms given as follows [19]:

$$\begin{aligned}F_1(\sigma) &= \frac{V_{FA}(\sigma)}{V_{FF}(\sigma)} + 1,\\ F_2(\sigma) &= \frac{S_{PB}(\sigma)}{S_{PT}(\sigma)} + 1.\end{aligned} \tag{10}$$

In the formula, $S_{FA}(\sigma), S_{FF}(\sigma)$ is the self-power spectral density function of acceleration and vibration load, and $V_{FA}(\sigma), V_{FF}(\sigma)$ is the cross-spectral density function of acceleration and vibration load. The specific calculation process is

$$\begin{aligned}V_{FA}(\sigma) &= \frac{1}{M_V^2}\left(\sum_{m=0}^{m_v-1} B(s)_m\right),\\ V_{FF}(\sigma) &= \frac{1}{M_v^2}\left(\sum_{m=0}^{M_v-1} V(s)_m e^{-2}\right)^2.\end{aligned} \tag{11}$$

In the formula, i is the narrative unit, e is the natural constant, and $F(S)_n$ is the measured vibration load.

In theory, when calculating the frequency response function, there are interferences such as noise during the measurement process. The influence of noise on the measured vibration load can be calculated as

$$\theta^2(\sigma) = \frac{V_{FA}(\sigma)V_{AA}(\sigma)}{V_{FF}(\sigma)V_{AF}(\sigma)}. \tag{12}$$

The coherence coefficient represents the correlation between the measured dynamic response and the applied load, and its amplitude is between 0 and 1. The higher the amplitude, the higher is the correlation between the dynamic response and the applied load. If the value is 1, it indicates that the measured dynamic response is completely caused by the applied vibration load, and the reliability of the result is the highest.

2.4. Elastic-Plastic Stress Distribution of the Surrounding Rock of the Tunnel. When the lateral pressure coefficient is $\varphi = 1$, it balances the initial stress in all directions of the surrounding rock and represents the state of axial load or hydrostatic pressure. The trend of the surrounding rock at a specific point must satisfy the balanced differential equation of the polar coordinate system.

$$\frac{\varphi_s}{\bar{\omega}_s} + \frac{1\varphi\pi_{r\varepsilon}}{s\varphi} + \frac{\varphi_s - \varphi_\varepsilon}{s} + Q_s = 0. \tag{13}$$

When $\varphi = 1$, assuming $Q_s = 0$, the radius of the plastic zone is the largest, where the stress concentration is the most serious, and the stress in the plastic zone has nothing to do with the original rock stress, and for the plastic zone, it can be simplified to

$$\frac{c\varphi_{sd}}{c_s} + \frac{\varphi_{sd} - \varphi_{\varepsilon d}}{s} = 0. \tag{14}$$

In the formula, φ_{sd} and $\varphi_{\varepsilon d}$ are the radial and tangential normal stresses in the plastic zone, respectively.

According to the Mohr-Coulomb criterion, the Mohr voltage cycle corresponding to the voltage state at any point on the plastic zone must be in contact with the strength shell. It must meet the following conditions:

$$\begin{cases} \varphi_{sd} = \dfrac{\varphi_c}{\lambda - 1}\left[\left(\dfrac{s}{s_a}\right)^{\lambda - 1} - 1\right], \\ \varphi_1 = \lambda\varphi_3 + \varphi_c. \end{cases} \tag{15}$$

From the abovementioned derivation, it can be analyzed that when $\varphi = 1$, the plastic structure of the surrounding rock appears on both sides of the cavern. The rock pillars between the crossing tunnels are usually larger than the rock pillars in the middle of the existing tunnel. The larger the radius of the plastic zone, the more concentrated is the stress.

3. Computer-Aided Analysis of the Dynamic Response Characteristics of the Surrounding Rock Structure of the Heavy-Duty Railway with a Small Clearance Crossing Tunnel

Crossing tunnels are typical geotechnical proximity projects. The construction of new tunnels will inevitably break the original rock-soil balance of in-situ stress and produce additional effects on the existing tunnel structure, affecting the safe operation and even the structure of the existing tunnel safety. The tunnel bottom structure is the main load-bearing structure of the heavy-duty railway of the grade-crossing tunnel, and the load size is mostly determined based on the experience of ordinary railway tunnels [20, 21]. The accurate theoretical calculation method can quickly calculate the dynamic load on the surface of each structural layer and determine the initial load conditions of the calculation model, which has important guiding significance for the design of heavy-duty railway tunnels [22, 23].

3.1. Experimental Methods and Procedures. In order to analyze the elastoplastic state of adjacent horizontal small-distance tunnels, the analytical solution of the penetration radius of the plastic zone of the surrounding rock of the small-distance tunnel is given, and the mutual influence between the two crossing tunnels is calculated. In order to analyze the dynamic response characteristics of the surrounding rock structure of the heavy-duty railway in the small clearance crossing tunnel, a computer-aided analysis block diagram of the dynamic response characteristics of the surrounding rock structure of the grade-crossing tunnel is presented in Figure 2.

The specific process of the test is as follows:

(1) Preliminary material preparation for the test includes the production of model tunnels, the preparation of model stratum materials, and the pretest of the equipment required for the test (whether the test equipment can work normally).

(2) After completing the model frame, the filling process can be roughly divided into three stages according to the filling height. The model soil at the bottom of the tunnel model is filled, the model soil at the top of the tunnel model is filled, and the model soil is filled to the final design height [24, 25]. Each filling process needs to be subdivided into multiple filling layers, and each filling layer must achieve a given degree of compression. The specific operation process is as follows. First, loosen the soil of a certain quality (calculated by dividing the expected filling amount by the density), then compact the whole with an I-beam, and finally hit the soil with a stone hammer. By controlling the number of boxes and the number of percussions, it is ensured that the planks at the corners of the model box are compressed to exceed the expected ground height [26, 27].

(3) We then carry out tunnel model embedment and acceleration sensor layout work. This stage and the previous stage are intersected. After completing the first filling stage, we place the tunnel model into the model box and then continue the subsequent filling process [28]. The burying of the acceleration sensor inside the soil is carried out layer by layer. The time for burying each layer is selected when the current soil layer height is greater than the buried depth of the measuring point by 5 cm. When burying, a small hole with a depth of 5 cm at the measuring point is

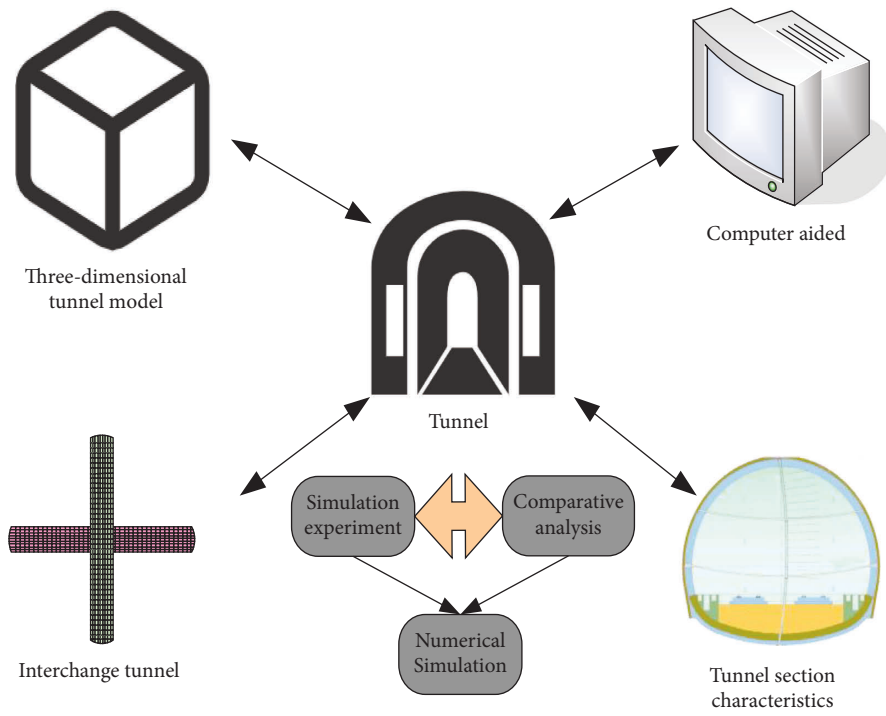

Figure 2: Frame diagram of the computer-aided analysis of dynamic response characteristics of the surrounding rock structure of the grade-crossing tunnel.

dug with a self-made tool, and then we bury the measuring point and finally fill it with compaction. The measuring points on the surface of the soil are laid directly after filling the model soil without drilling holes [29, 30].

(4) We then carry out the wiring of test equipment and carry out specific test work. The test is divided into three groups according to the type of applied load: fixed frequency sinusoidal vibration load, swept frequency vibration load, and train vibration load. Among them, the sinusoidal vibration load frequency is set to 60 Hz, 120 Hz, and 180 Hz, and the dynamic response under 3 kinds of amplitudes (excitation voltages are 800 mV, 1000 mV, and 1200 mV, respectively) is tested at the same time. The sweep frequency vibration load tests the dynamic response under 3 kinds of frequency sweep cycles, 2 kinds of frequency directions, and 3 kinds of excitation voltage, and the test time of each group is guaranteed to be more than 3 times of the frequency sweep cycle. The test time of each group of train vibration loads is also guaranteed to be more than 3 cycles.

This article uses computer-aided analysis, and the computer-aided analysis process is shown in Figure 3.

The computer-aided information analysis system consists of four parts: the database, the information analysis method, and the information analysis software and information analysis staff. Among them, the database is the foundation, and the database resources of the database system are the objects of information analysis. Information analysis methods are tools, and choosing mature, logical, and effective methods is an important prerequisite for information analysis.

3.2. Surrounding Rock Materials. In the process of designing the model test, considering that the overall rock is less affected by scouring during the short test period, it is difficult to have an ideal void form during the test, so it was decided to study the soil surrounding the rock as the object. According to the "Code for Design of Foundations for Buildings" (GB50007-2011), soil (including rocks) can be divided into six categories, namely rock, gravel soil, sand, silt, cohesive soil, and artificial fill. According to the geotechnical classification standard for railway engineering (tb10077-2001), general soil can be divided into gravel soil, sandy soil, silt, and cohesive soil. The structural model of the tunnel bottom is simplified to a certain extent. The inverted arch filling and inverted arch structure are regarded as a whole structure, and the gypsum material is used for prefabrication, as shown in Table 1.

The process of groundwater erosion on the surrounding rock at the bottom of the heavy-duty railway tunnel structure due to the dynamic load of the heavy-duty train is studied. The qualitative analysis of the three types of soil surrounding the rocks: pebble soil, cohesive soil, and sandy soil is carried out. The form of voids and the distribution characteristics of voids appeared during the long-term erosion of groundwater, and the distribution of contact pressure and Earth pressure at the bottom of the tunnel is quantitatively studied. The gravity, strength, and deformation characteristics of similar materials that simulate the

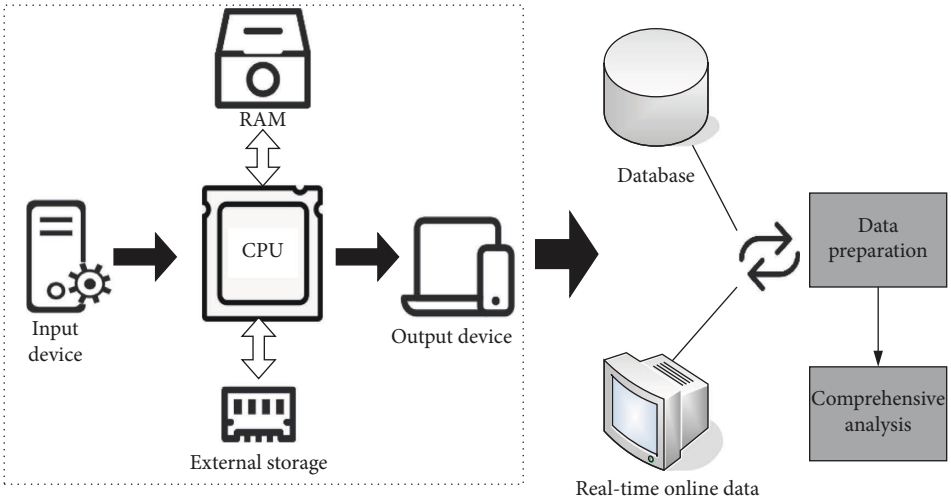

Figure 3: Computer-aided analysis process.

Table 1: Surrounding rock material.

Category	Soil name	Classification standard	Particle size (mm)	Specification
Gravel soil	Boulder soil/rock soil/pebble soil	Gradation of soil particles	>200/20/2	50%
Sandy soil	Gravel/coarse sand/nakasago/fine sand	Gradation of soil particles	>0.5/0.25/0.075	50%/85%
Silt	Silt	—	>0.075	Plasticity index ≤10
Clay soil	Silty clay/clay	Plasticity index	$10 < Ip \leq 17$	

surrounding rock must meet the geomechanical similarity requirements. We then determine the value range of the physical and mechanical parameters of the surrounding rock model material, as shown in Table 2.

When simulating cohesive soil, sandy soil, and sandy gravel soil under V-level surrounding rock conditions, the mechanical parameters of similar materials should meet the value range in Table 2 as much as possible.

Table 2: Material parameters of the surrounding rock model.

Class V surrounding rock	Prototype	Model
Severe	17–20	17–20
Deformation modulus	1000–2000	50–100
Poisson's ratio	0.35–0.45	0.35–0.45
Internal friction angle	20–27	20–27
Cohesion	50–200	2.5–10

4. Computer-Aided Analysis of the Dynamic Response Characteristics of the Surrounding Rock Structure of the Heavy-Duty Railway with Small Clearance Crossing Tunnels

4.1. Dynamic Response Characteristics of The Surrounding Rock Structure. Because the train connectivity has strict requirements on the vertical displacement of the track, the maximum vertical vibration displacement response value at the cross-tunnel track bed structure of the three-dimensional crossing tunnel is taken as the numerical value of the study.

It can be seen from Tables 3 and 4 that the grade-crossing tunnels at different train speeds and at different clear distances affect the partitions along the track direction.

With the increase in train speed, the distance between the strong and weak affected areas and the intersection is increased, but the increase in the distance is not very obvious. Under the action of the downward train load, it will affect the displacement and acceleration response of the observation points of the conventional section of the upper-span tunnel. Although smaller, it will have a certain impact on the interchange section. Among them, the influence of the downstream train load on the maximum vertical displacement and the maximum acceleration response of the overpass tunnel is smaller than the influence of the upward train load on the maximum vertical displacement of the underpass tunnel.

It can be seen from the different clear distance divisions that the tunnel clear distance has a greater impact on the maximum vertical displacement of the track bed. When the clear distance exceeds 25 m, there is only a certain range of weakly affected areas along the track direction. Under the load of the upper and lower crossing trains, the influence of the displacement and acceleration response of each observation point of the upper and lower cross-section will increase to a certain extent. Compared with the upward load, for the upper-span tunnel, the maximum downward vertical displacement of the track bed has increased by 30.2%, and the acceleration has increased by 0.16 m/s^2.

4.2. Simulation of the Indoor Model Experiment Analysis. Using indoor model testing and finite element numerical simulation, the process of groundwater scouring the surrounding rock at the bottom of a heavy-duty railway tunnel

Table 3: Influence of different train speeds on the division of track direction.

Train speed (km/h)	Influence zone			
	Destruction zone	Strong influence zone (W)	Weak impact zone (W)	Unaffected zone (W)
260	—	0~0.67	0.67~1.4	>1.4
230	—	0~0.87	0.87~1.6	>1.6
360	0~0.27 W	0.27~1	1~1.8	>1.8

Table 4: The effect of different clear distances on the area division along the track.

Clear distance (m)	Influence zone			
	Destruction zone	Strong influence zone	Weak impact zone (W)	Unaffected zone (W)
5	0~0.27 W	0.27~0.67 W	0.67~1.8	>1.8
10	—	0~0.87 W	0.87~1.6	>1.6
15	—	0~0.73 W	0.73~1.6	>1.6
20	—	—	0~1.13	>1.13

bottom structure due to the dynamic load of a heavy-duty train during operation is studied, and the variation law of contact pressure and the transmission characteristics of Earth pressure under void state are quantitatively analyzed.

In order to reflect the contact pressure distribution under the floor structure, the maximum value of the contact pressure of the three surrounding rock materials was extracted. The change curve of the contact pressure when there is water and when there is no water is shown in Figure 4.

When the surrounding rock at the bottom of the tunnel is in a water-rich condition, the additional value of the contact pressure at the two measuring points below the center line and the bottom left decreases slightly during the excitation process.

As shown in Figure 5, when the surrounding rock of the sandy soil at the bottom of the tunnel is in anhydrous conditions, the additional value of the contact pressure at the measurement points below the center line and the bottom left of the center line increases with the change in the excitation time. The distribution pattern of the sandy soil surrounding the rock after vibration is the same. The appearance of the hard soil block on the right side of the center line indicates that this location will bear greater stress, while other parts of the surrounding rock are continuously weakened by scouring due to pumping action. As a result, the contact pressure is becoming smaller and smaller.

The relationship between the model parameters and the selectable granular material parameters is established through corresponding numerical simulation experiments. This process is usually called calibration. The simulation of the numerical test is roughly divided into three steps: sample generation, consolidation, and loading. The model is surrounded by 4 walls; the upper and lower walls simulate the loading of the sample, and the four lateral walls are used to simulate the confining pressure. The loading of the sample is simulated by controlling the moving speed of the upper and lower walls. During the entire experiment, the speed of all lateral walls is automatically controlled by the servo mechanism to keep the confining pressure at a certain value.

The hydrodynamic pressure at the bottom of the tunnel is the main factor affecting the rate of erosion and deterioration of the surrounding rock, so it is a key parameter in the numerical calculation and analysis. However, the actual hydrodynamic pressure changes continuously with geological conditions and train operations and involves complex fluid-solid coupling and mechanical principles. Therefore, the hydrodynamic pressure value in the particle flow calculation is mainly based on onsite monitoring data. As shown in Figure 6.

According to the time history curve of invert pore water pressure obtained from field monitoring, the pore water pressure at each part of the tunnel bottom increases in varying degrees. The increase of pore water pressure at the bottom of the right ditch is the most obvious, with great added value; the pore water pressure at the left arch foot and right rail increases moderately. The long-term monitoring data show that the pore water pressure under the tunnel inverted arch still continues to increase one year after opening to traffic.

4.3. Vibration Load Analysis of a Small Clearance Intersecting Tunnel. Different sections of the tunnel lining structure have different effects on the dynamic response of different parts. To analyze the vertical vibration displacement, vibration acceleration, and principal stress of key parts of the tunnel lining structure, this study uses swept frequency vibration load and frequency response function (FRF) to obtain the dynamic response characteristics at different vibration frequencies and analyzes the reliability of the model test results. Due to the large fluctuation of the FRF curve, this study uses the 1/3 octave method to further process the vertical acceleration response results of the lining structure. 1/3 octave divides a given frequency range into successive bands using a constant percentage bandwidth, each band has an upper center frequency, and the ratio of the center frequencies to the lower band remains unchanged.

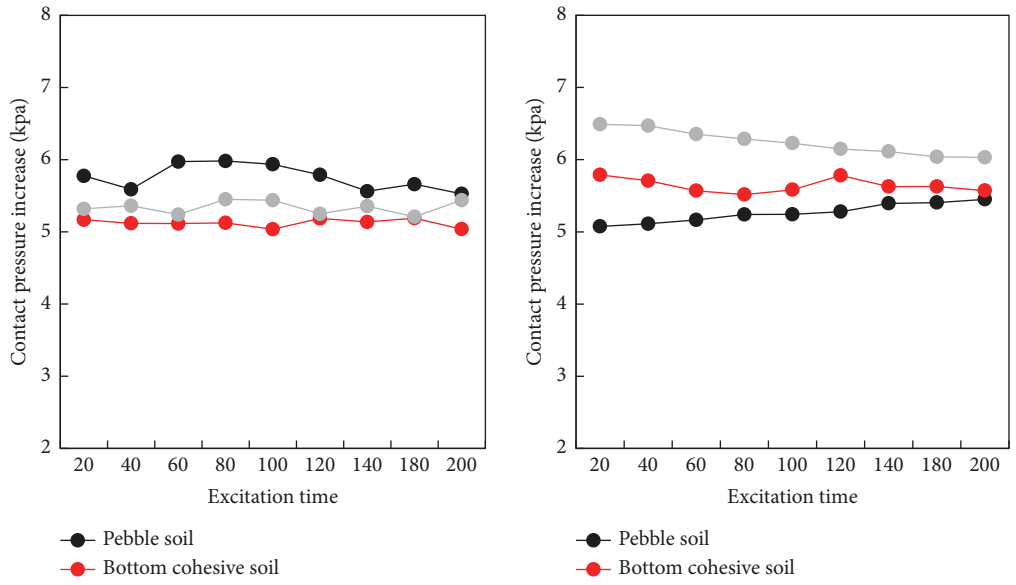

Figure 4: Change curve of the additional value of contact pressure when there is water.

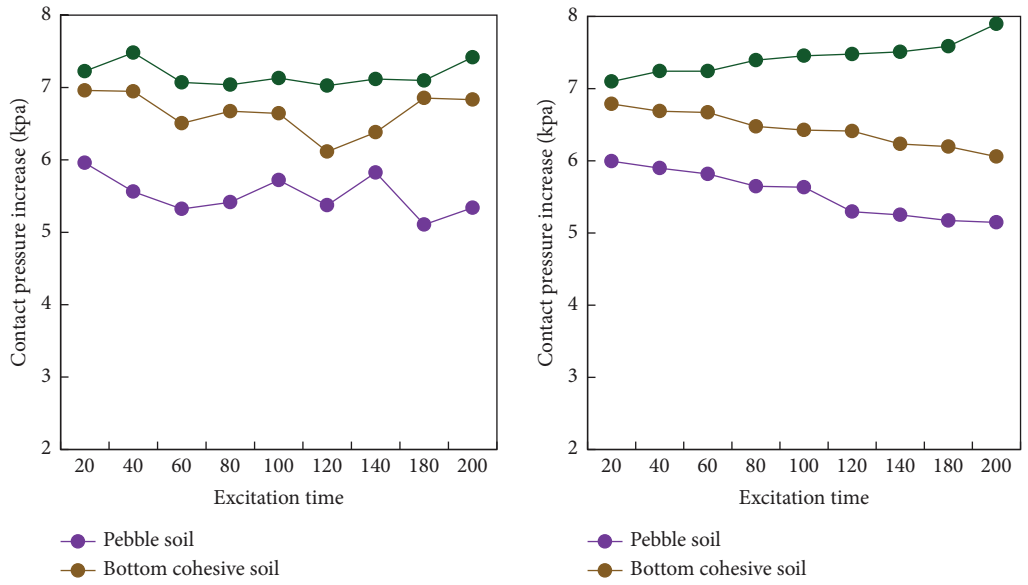

Figure 5: Change curve of the additional value of contact pressure when there is no water.

The frequency range of this research is 0~250 Hz, and the corresponding center frequency and frequency range of each frequency band of 1/3 octave is shown in Table 5.

In order to deeply analyze the dynamic response characteristics of the ground surrounding the tunnel under different frequency loads, and to eliminate the influence of the vibration load amplitude on the results, the frequency response function is used to process the results.

The applied train vibration load is obtained through the collection. During the analysis, based on the vehicle track coupling dynamics theory, first the vehicle and track model are established separately, and then the interaction between wheel and rail is comprehensively considered. Finally, the train vibration load acting on the track bed is obtained. In the vehicle model, the vehicle suspension system is simplified as a wheelset sprung mass system, which is developed into a complete vehicle model with two series. The degree of freedom of the model is 10, and the system equation can be obtained by applying the D'Alembert principle to each rigid body one by one. The rail is simplified as the Euler beam model in the track model. Although the influence of shear force and moment of inertia is ignored, it has high accuracy in calculating vertical vibration below 500 Hz. At the same time, considering the influence of track fasteners, the tunnel and monolithic track bed are considered as continuous foundation conditions. The interaction between wheel and rail mainly considers the influence of track irregularity. In the literature, 6-level track spectral density based on the

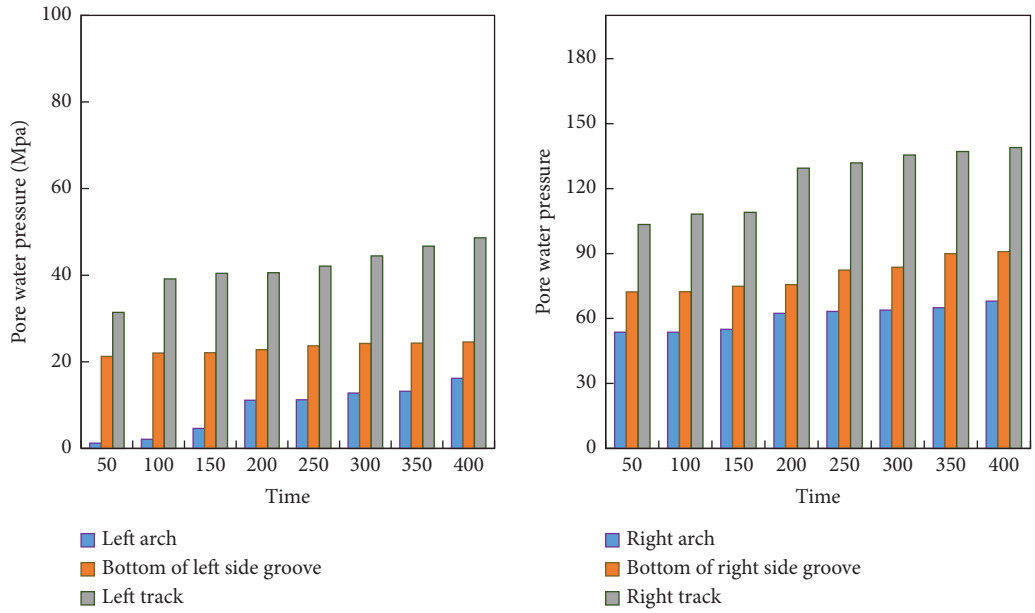

Figure 6: time history curve of invert pore water pressure.

Table 5: Center frequency and frequency range.

Center frequency	Frequency range	Center frequency	Frequency range
1.25	1.41~1.78	10	7.18~9.01
2.5	1.78~2.44	12.5	9.01~12.2
3.75	2.45~2.92	15	12.2~15.1
5	2.92~3.65	17.5	15.1~23.4
6.25	3.65~4.57	20	23.4~29.2
7.5	4.57~5.72	22.5	29.2~36.5
8.65	5.72~7.18	25	36.5~44.7

American track spectrum is selected to analyze and simulate track irregularity, and only high and low irregularity are considered. The corresponding speed of the simulated train vibration load is 80 km/h, and the load time history curve is shown in Figure 7.

Compared with the tunnel structure, the ground acceleration response under the moving train load is obviously weaker, and it is mainly concentrated in the ground adjacent to the tunnel. The decay rate of the acceleration response of the formation in the horizontal direction is obviously greater than that in the vertical direction. When considering segment joints, the calculation result of formation acceleration response is generally too large.

Through Fourier transform, the time domain results measured under fixed frequency sinusoidal load and swept frequency vibration load can be converted into the frequency domain, and the dynamic response characteristics of the lining structure and the ground under different load frequencies can be obtained. Applying train vibration load can directly obtain the response characteristics of the model in the time domain. This hypothesis is verified by applying sinusoidal vibration loads of different amplitudes. The excitation force curve under the two excitation voltages is shown in Figure 8.

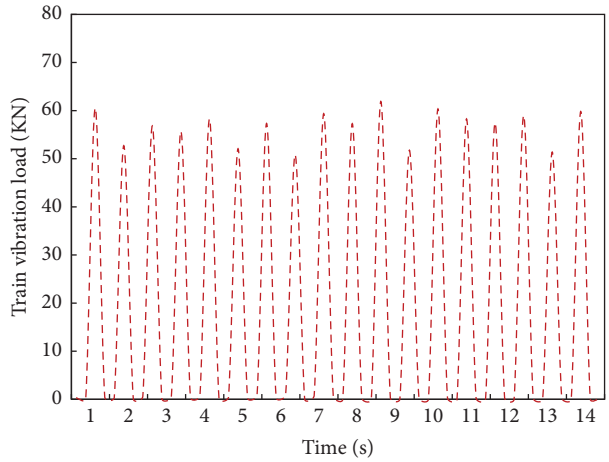

Figure 7: Train vibration load at a speed of 80 km/h.

The amplitude of the excitation force is different under different excitation voltages. The greater the excitation voltage, the greater is the excitation force. Under the same excitation voltage, the excitation force is different under different vibration frequencies. The dynamic response amplitude of the lining structure and the surrounding ground under different excitation voltages are also different. The dynamic response amplitude increases with the increase of the excitation voltage. At the same monitoring point, the dynamic response amplitudes under the same excitation voltage and different vibration frequencies are different, reflecting that the dynamic response is not only related to the load amplitude but also to the frequency of the vibration load.

The coherence coefficient represents the correlation between the measured dynamic response and the applied load, and its amplitude is between 0 and 1. The higher the amplitude, the higher the correlation between the dynamic

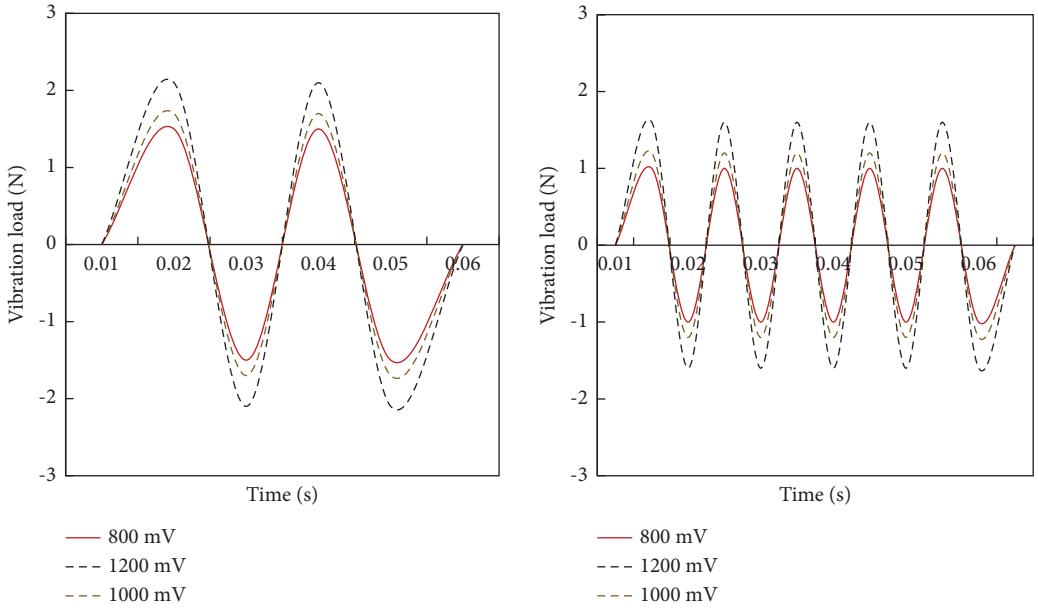

Figure 8: Time history curve of excitation force under different excitation voltages.

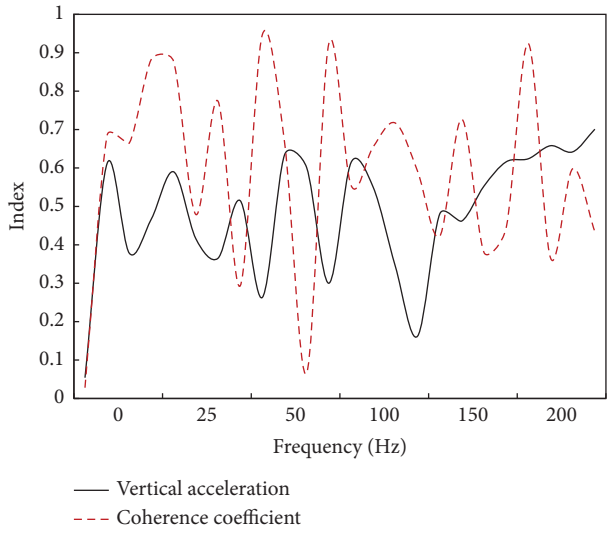

Figure 9: Frequency response function and correlation coefficient under 60 Hz.

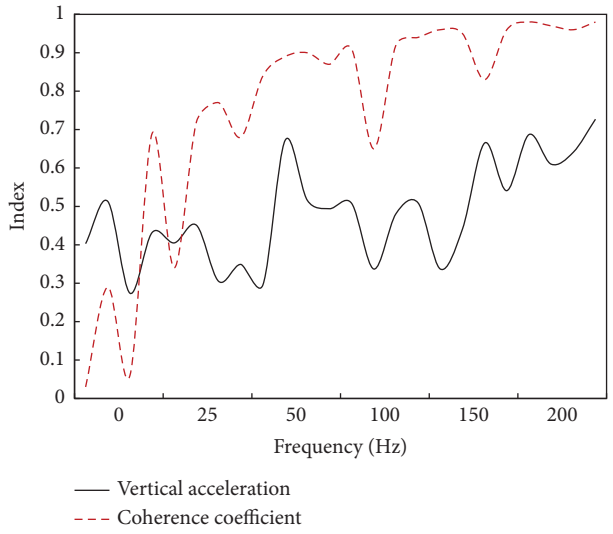

Figure 10: Frequency response function and correlation coefficient under 120 Hz.

response and the applied load. If the value is 1, it indicates that the measured dynamic response is completely caused by the applied vibration load, and the reliability of the result is the highest. It can be seen from Figures 9 and 10 that when the vibration frequency is below 50 Hz, the coherence coefficient of the formation dynamic response is small and the fluctuation changes significantly, indicating that the reliability of the frequency response function results in this frequency range is low as a whole. When the vibration load is in the frequency range of 50–100 Hz, the coherence coefficient is generally high, but there are also obvious fluctuations, but the overall trend shows a gradual increase with the increase of frequency. When the vibration frequency exceeds 100 Hz, the coherence coefficient is basically close to 1, indicating that the frequency response function response results in this section are the most reliable. At the same time, the difference in formation dynamic response measured under the two loads is small, which shows that the reliability of the formation test results under swept frequency vibration load is high.

5. Conclusions

In this study, the dynamic response characteristics of surrounding rock structures of heavy haul railways in small clear-distance interchange tunnels are analyzed by computer-aided under intelligent manufacturing. The following results are obtained, including dividing the heavy-duty railway tunnel into upper arch wall structure and lower tunnel bottom structure by analyzing the dynamic response

and stress distribution characteristics, respectively. The increase in the axle load of heavy haul trains, the decrease of surrounding rock conditions, and the reduction of distance from the active position of train load will increase the dynamic load increment and structural internal force on the structural surface, thus clarifying the surface load distribution and vertical transmission law of each structural layer of the tunnel bottom structure of heavy haul railway tunnel. The load of the heavy-duty train gradually decreases with the increase of the vertical depth during the transmission process of the tunnel bottom structure. The large rigidity of the track bed structure and the large thickness of the filling layer have a buffer effect on the dynamic load. In this study, some achievements have been made through the research on the dynamic response characteristics of the heavy-duty railway surrounding the rock structure of the interchange tunnel, but there are still some deficiencies. For example, in the process of analyzing the surrounding rock structure at the bottom of the tunnel, several common surrounding rock materials are mainly considered, and other surrounding rock materials are not analyzed. In this study, specifically, the three-dimensional dynamic numerical simulation calculation is used to study the influence of the dynamic characteristics of different sections of the grade separation tunnel under different working conditions, but the numerical simulation method is still different from the actual situation which needs to be further improved.

Data Availability

The data supporting the current study are given in the article.

Conflicts of Interest

The authors declare that they have no conflicts of interest.

References

[1] J. Lv, X. Li, Z. Li, and H Fu, "Numerical simulations of construction of shield tunnel with small clearance to adjacent tunnel without and with isolation pile reinforcement," *KSCE Journal of Civil Engineering*, vol. 24, no. 1, pp. 295–309, 2020.

[2] X. Liu, Q. Fang, and D. Zhang, "Mechanical responses of existing tunnel due to new tunnelling below without clearance," *Tunnelling and Underground Space Technology*, vol. 80, pp. 44–52, 2018.

[3] R. R. Al-Omari, A. A. Al-Azzawi, and K. A. Alabbas, "Behavior of piled rafts overlying a tunnel in sandy soil," *Geomechanics and Engineering*, vol. 10, no. 5, pp. 599–615, 2016.

[4] D. M. Zhang, Z. K. Huang, Z. L. Li, X. Zong, and D. M Zhang, "Analytical solution for the response of an existing tunnel to a new tunnel excavation underneath," *Computers and Geotechnics*, vol. 108, pp. 197–211, 2019.

[5] Y. X. Xiao, X. T. Feng, G. L. Feng, H. J. Liu, Q. Jiang, and S. L Qiu, "Mechanism of evolution of stress–structure controlled collapse of surrounding rock in caverns: a case study from the Baihetan hydropower station in China," *Tunnelling and Underground Space Technology*, vol. 51, pp. 56–67, 2016.

[6] M. He, S. Chen, and Z. Guo, "Control of surrounding rock structure for gob-side entry retaining by cutting roof to release pressure and its engineering application[J]," *Zhongguo Kuangye Daxue Xuebao/Journal of China University of Mining and Technology*, vol. 46, no. 5, pp. 959–969, 2017.

[7] S. H. Chen, H. U. Shuai-Wei, and Z. H. Zhang, "Propagation characteristics of vibration waves induced in surrounding rock by tunneling blasting[J]," *Journal of Mountain Science*, vol. 2017, no. 12, pp. 269–279, 2017.

[8] G. Li, C. Wang, and G. Wang, "Effect of the blocking water and limiting discharge and surrounding rock permeability on the stability of subsea tunnel[J]," *Geotechnical & Geological Engineering*, vol. 39, no. 1998, pp. 1–16, 2021.

[9] G. Wang and Y. Pang, "Surrounding rock control theory and longwall mining technology innovation," *International Journal of Coal Science & Technology*, vol. 4, no. 4, pp. 301–309, 2017.

[10] F. Huang, M. Zhang, and F. Wang, "The failure mechanism of surrounding rock around an existing shield tunnel induced by an adjacent excavation[J]," *Computers and Geotechnics*, vol. 117, pp. 103236.1–103236.11, 2020.

[11] Z. Fang, Z. Zhu, and P. Wu, "Excavation and support method of tunnel with high ground stress and weak surrounding rock based on GIS[J]," *Arabian Journal of Geosciences*, vol. 14, no. 7, pp. 1–13, 2021.

[12] Z. Jiachen Wang, "Systematic principles of surrounding rock control in longwall mining within thick coal seams[J]," *International Journal of Mining Science and Technology*, vol. 29, no. 01, pp. 64–70, 2019.

[13] P. Liu, S. Cui, Z. Li, X. Xu, and C Guo, "Influence of surrounding rock temperature on mechanical property and pore structure of concrete for shotcrete use in a hot-dry environment of high-temperature geothermal tunnel," *Construction and Building Materials*, vol. 207, no. 20, pp. 329–337, 2019.

[14] B. U. Qingwei, Y. Xin, and C. Wang, "Stability analysis on bearing structure in the surrounding rock between staggered roadways[J]," *Meitan Xuebao/Journal of the China Coal Society*, vol. 43, no. 7, pp. 1866–1877, 2018.

[15] J. Kan, J. Wu, and N. Zhang, "Structure stability analysis and control technology of surrounding rock ofthe secondary gob-side entry retaining[J]," *Caikuang Yu Anquan Gongcheng Xuebao/journal of Mining & Safety Engineering*, vol. 35, no. 5, pp. 877–884, 2018.

[16] M. Buri, "Dynamic clearance analysis paves way for automated fleet[J]," *Railway Gazette International*, vol. 174, no. 3, pp. 41–43, 2018.

[17] G. S. Dhaliwal and G. M. Newaz, "Effect of layer structure on dynamic response and failure characteristics of carbon fiber reinforced aluminum laminates (CARALL)," *Journal of Dynamic Behavior of Materials*, vol. 2, no. 3, pp. 399–409, 2016.

[18] K. Y. Kang, K. H. Choi, J. W. Choi, Y. Ryu, and J. M Lee, "Dynamic response of structural models according to characteristics of gas explosion on topside platform," *Ocean Engineering*, vol. 113, no. 1, pp. 174–190, 2016.

[19] A. Fenerci, O. Oiseth, and A. Ronnquist, "Long-term monitoring of wind field characteristics and dynamic response of a long-span suspension bridge in complex terrain," *Engineering Structures*, vol. 147, no. 15, pp. 269–284, 2017.

[20] X. Wang, G. Liu, S. Ma, and R Tong, "Effects of restitution coefficient and material characteristics on dynamic response of planar multi-body systems with revolute clearance joint," *Journal of Mechanical Science and Technology*, vol. 31, no. 2, pp. 587–597, 2017.

[21] Pu, Xiaowu, and Wang, "Study of shaking table test on dynamic response characteristics and failure mechanism of the

loess slope[J]," *Earthquake Research in China*, vol. 34, no. 01, pp. 128–142, 2020.

[22] T. Zhao, W. Wang, Z. Chen et al., "Dynamic response characteristics of 93W alloy with a spherical structure," *Open Physics*, vol. 18, no. 1, pp. 199–211, 2020.

[23] X. Zhai, S. Wu, K. Wang, X. Chen, and H Li, "A novel design of rescue capsule considering the pressure characteristics and thermal dynamic response with thermomechanical coupling action subjected to gas explosion load," *Shock and Vibration*, vol. 2017, no. 4, pp. 1–12, 2017.

[24] V. B. Maji, "Dynamic Response Characteristics of Hollow Steel Single Pile under Vertical Excitations[J]," *Lecture Notes in Civil Engineering] Geotechnical Applications*, vol. 13, no. 4, pp. 33–40, 2019.

[25] H. Chen, Q. Yan, and W. Chen, "Seismic dynamic response characteristics of slope in small diameter bias double tunnels [J]," *International Journal of Applied Environmental Sciences*, vol. 12, no. 3, pp. 513–525, 2017.

[26] Q. A. Bhatti, "Dynamic response characteristics of steel portal frames having semi-rigid joints under sinusoidal wave excitation[J]," *International Journal of Advanced Structural Engineering*, vol. 9, no. 4, pp. 1–5, 2017.

[27] X. Jiang, W. Liu, H. Yang, J. Zhang, and L Yu, "Study on dynamic response characteristics of slope with double-arch tunnel under seismic action," *Geotechnical & Geological Engineering*, vol. 39, no. 2, pp. 1349–1363, 2021.

[28] Z. Yuan, W. Liu, and M. Ye, "A mapping method of dynamic response and stiffness characteristics for realizing a customized nonlinear oscillator," *Nonlinear Dynamics*, vol. 102, no. 4, pp. 2531–2548, 2020.

[29] J. R. Cho, S. Y. Lee, and M. S. Song, "Dynamic response characteristics of cylindrical baffled liquid storage tank to the baffle number," *Journal of Mechanical Science and Technology*, vol. 33, no. 12, pp. 5979–5987, 2019.

[30] A. Ys, G. A. Rui, and B. Xw, "Dynamic response characteristics of permeable asphalt pavement based on unsaturated seepage - ScienceDirect," *International Journal of Transportation Science and Technology*, vol. 8, no. 4, pp. 403–417, 2019.